

Referring Camouflaged Object Detection

Xuying Zhang, Bowen Yin, Zheng Lin, Qibin Hou, *Member, IEEE*,
Deng-Ping Fan, *Senior Member, IEEE*, Ming-Ming Cheng, *Senior Member, IEEE*

Abstract—We consider the problem of referring camouflaged object detection (Ref-COD), a new task that aims to segment specified camouflaged objects based on a small set of referring images with salient target objects. We first assemble a large-scale dataset, called R2C7K, which consists of 7K images covering 64 object categories in real-world scenarios. Then, we develop a simple but strong dual-branch framework, dubbed R2CNet, with a reference branch embedding the common representations of target objects from referring images and a segmentation branch identifying and segmenting camouflaged objects under the guidance of the common representations. In particular, we design a Referring Mask Generation module to generate pixel-level prior mask and a Referring Feature Enrichment module to enhance the capability of identifying specified camouflaged objects. Extensive experiments show the superiority of our Ref-COD methods over their COD counterparts in segmenting specified camouflaged objects and identifying the main body of target objects. Our code and dataset are publicly available at <https://github.com/zhangxuying1004/RefCOD>.

Index Terms—Referring Camouflaged Object Detection; Common Representations; R2C7K Dataset; R2CNet Framework.

1 INTRODUCTION

CAMOUFLAGED object detection (COD), which aims to segment objects that are visually hidden in their surroundings, has been attracting more and more attentions [1], [2], [3], [4]. This research topic plays an important role in a wide range of real-world applications, *e.g.*, medical image segmentation [5], [6], surface defect detection [7], [8], and pest detection [9]. It is noteworthy that although there may be multiple camouflaged objects in a real scene, we just want to find the specified ones in many applications. A typical example should be the explorers are looking for some special species but most of them may be hidden deep together with other similar objects. In this case, if we have some references about the targets, the finding process will become orientable and thus get easier. As a result, it is promising to explore the COD research with references, which is abbreviated as Ref-COD in this paper.

Ref-COD leverages the referring information to guide the identification of specified camouflaged objects, which is consistent with that of human visual perception to camouflaged objects [10]. And the key issue lies on which form of information is appropriate to be used as a reference. Recent works have explored several forms of reference for image segmentation, *e.g.*, referring expression segmentation with text reference [11], and few-shot segmentation with image reference [12]. However, whether the annotated images containing specified camouflaged objects or detailed textual descriptions of camouflaged objects for existing images, the acquisition process is time-consuming and laborious, which hinders the transfer of these methods to COD. Considering that images with salient objects are readily available on the Internet, a straightforward question arises: Is it possible for us to take advantage of such images to help better identify specified camouflaged objects?

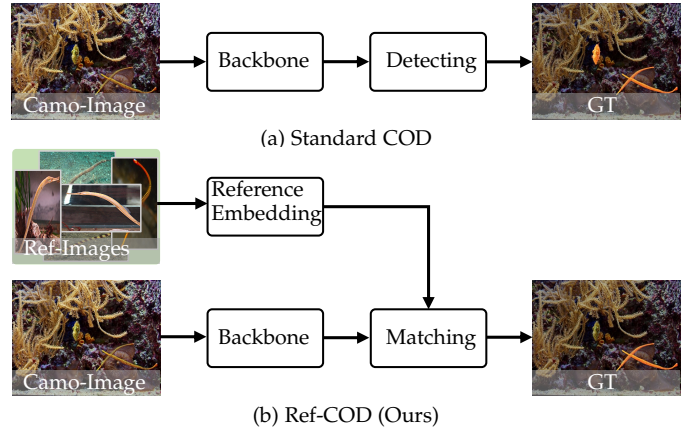


Fig. 1. Visual comparison between the standard COD and our Ref-COD. Given an image containing multiple camouflaged objects, the COD model tends to find all possible camouflaged objects that are blended into the background without discrimination, while the Ref-COD model attempts to identify the specified camouflaged objects under the condition of a set of referring images.

Motivated by this question, we propose a novel Ref-COD benchmark. Our intention is to leverage the increasingly advanced research on salient object detection (SOD) to acquire common representations of target objects from referring images, which are used to guide the segmentation of specified camouflaged objects. Fig. 1 illustrates the task relationship between the standard COD and our Ref-COD. In particular, our Ref-COD transforms the process of COD from detecting aimlessly the differential objects in camouflage scenes to matching target objects with specified purposes. To enable a comprehensive study on this new benchmark, we build a large-scale dataset, named R2C7K, which contains a large number of samples without copyright disputes in real-world scenarios. The basic information of this dataset is as follows: 1) It has 7K images covering 64 object categories; 2) It consists of two subsets, *i.e.*, the Camo-

- All the authors are with VCIP, School of Computer Science, Nankai University, Tianjin, China (zhangxuying1004@gmail.com).
- First two authors contributed equally.
- Q. Hou is the corresponding author (andrewhoux@gmail.com).

subset composed of images containing camouflaged objects and the Ref-subset composed of images containing salient objects; 3) The number of images for each category in the Ref-subset is fixed, while the one in the Camo-subset is not.

To investigate the role of the referring information in Ref-COD, we design a dual-branch network architecture and develop a simple but effective framework, named *R2CNet*. This framework includes a reference branch and a segmentation branch. The reference branch aims to capture common representations of target objects from the referring images composed of salient objects, which will be used to identify the specified camouflaged objects. Particularly, we build a Referring Mask Generation (RMG) module to generate pixel-level referring information. In this module, a dense comparison is performed between the common representations from the reference branch and each position of the visual features from the segmentation branch to generate a referring prior mask. However, there may exist variances in appearance between the camouflaged objects and the salient objects even though they belong to the same category, which may increase the difficulty of identifying accurate camouflaged objects. To overcome this shortcoming, a dual-source information fusion strategy is employed to eliminate the information differences between two information sources. In addition, we also design a Referring Feature Enrichment (RFE) module to achieve the interaction among multi-scale visual features under the guidance of referring mask, and further highlight the target objects.

Extensive experiments are conducted to validate the effectiveness of our Ref-COD. To be specific, we choose the segmentation branch with multi-scale feature fusion based on feature pyramid network (FPN) [13] as the baseline COD model, and compare it with our R2CNet in terms of the common metrics [14], [15], [16], [17] of COD research on the R2C7K dataset. Remarkably, our R2CNet outperforms the baseline model by a large margin. Furthermore, we also apply the design of Ref-COD on recent 7 state-of-the-art COD methods, and the Ref-COD methods consistently surpass their COD counterparts without bells and whistles. Besides, the visualization results also show quality predictions of the Ref-COD methods (e.g., R2CNet) in the segmentation of specified objects and the identification of the main body of camouflaged objects over the COD model (e.g., baseline).

To sum up, the contributions of this paper can be summarized as follows:

- We propose a new benchmark, termed Ref-COD. To the best of our knowledge, it is the first attempt to bridge SOD and COD and segment the specified camouflaged objects with salient object images.
- We build a large-scale dataset, named R2C7K, which could help provide data basis and deeper insights for the Ref-COD research.
- We design a new framework for Ref-COD research, dubbed R2CNet, whose excellent experimental results suggest that it could offer an effective solution to this novel topic.

2 RELATED WORK

In this section, we first present the research progress and existing problems of COD tasks. Then, we introduce the

development history of the SOD topic. Finally, we describe referring object segmentation research with different forms of reference information.

2.1 Camouflaged Object Detection

Identifying camouflaged objects from a confusing scene is challenging due to the high similarity to their surroundings, diversity in scale, fuzziness in appearance, *etc.* To solve this task, an increasing number of works have been proposed. One of the early systematic studies is presented by [18], which publishes a large-scale dataset with high-quality annotation, namely COD10K, and a well-designed search and identify framework for this research. Later on, a large number of strategies, *e.g.*, multi-scale feature fusion [2], [19], [20], [21], [22], multi-stage refinement [1], [23], [24], [25], graph learning [26], weakly supervised [27], uncertainty [28], [29], [30], foreground and background separation [31], [32], [33], and attention mechanism [34], [35] have been proposed to improve the performance of the COD models. More related works are presented in recent survey paper [36]. More recently, numerous works introduce additional information, *e.g.*, boundary [4], [37], [38], [39], [40], texture [3], [41], [42], frequency [43], [44], and depth [45], [46], [47], [47], as guidance to further improve the accuracy of the segmentation results. However, obtaining these forms of information of high quality from the existing camouflaged images requires expensive time and resource costs, and they cannot explicitly tell the COD model what to segment.

In this paper, we propose a novel benchmark, which extracts common representations of target objects from readily available referring images as explicit semantic guidance to locate and segment the specified camouflaged objects. This makes our work quite different from the standard COD task.

2.2 Salient Object Detection

Salient object detection (SOD) aims to capture the most attention-grabbing objects in the given image. The development of this topic has witnessed two stages: 1) the traditional method stage and 2) the deep learning method stage. During the former period, hand-crafted features [48], [49], [50], [51] from image patches, object proposals, and super-pixels, play the most important role. Although these methods work well in some scenes, the extraction of these features is usually time-consuming. More importantly, their performance may sharply degrade in complex conditions. With the prosperity of fully convolutional networks [52] and Transformers [53], [54], [55], [56], SOD research enters the latter stage. In this stage, U-shape structure [13], [57], multi-stage supervision [58], [59], [60], and attention mechanisms [61], [62] are widely used in SOD methods to achieve more accurate pixel-wise predictions.

It is worth mentioning that SOD has extensive applications in various research communities, *e.g.*, visual tracking [63], unsupervised segmentation [64], image compression [65], and content-aware image editing [66], mainly because it can help find the objects or regions that can efficiently represent a scene. This property of SOD also inspires the reference idea of this paper.

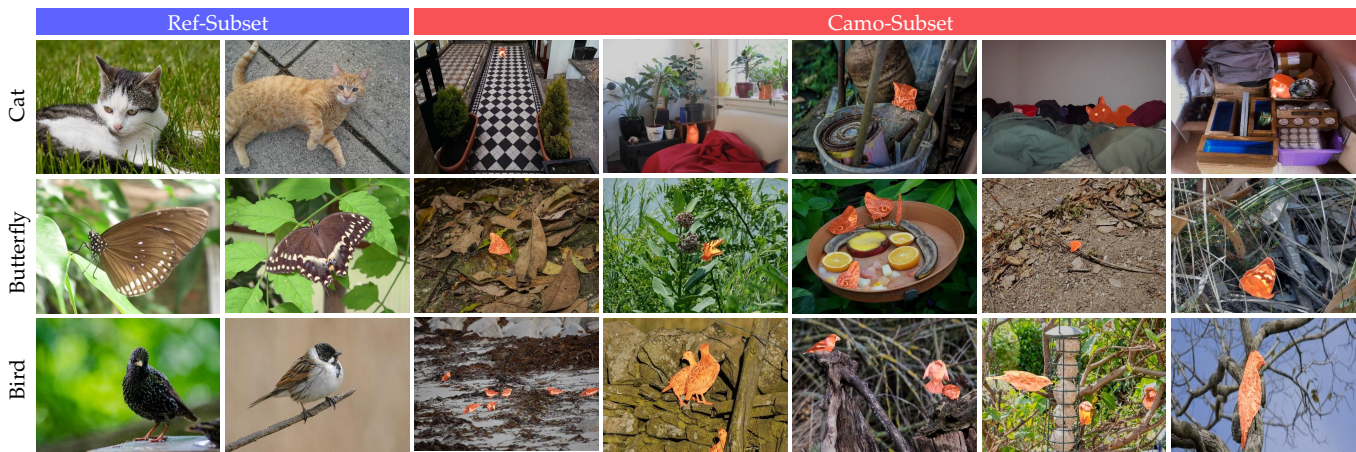


Fig. 2. Examples from our R2C7K dataset. Note that the camouflaged objects in Camo-subset are masked with their annotations in orange.

2.3 Referring Object Segmentation

Referring Object Segmentation means segmenting visual objects from a given image under a certain form of references, *e.g.*, image and text.

Few-shot segmentation (FSS) explores object segmentation guided by annotated images containing objects of the same category. The models are trained on a large number of images whose pixels are labeled with base classes (query set) and perform dense pixel prediction on unseen classes given a few annotated samples (support set). Particularly, most existing FSS networks include two branches, *i.e.*, support branch and query branch, to extract the features of support images and query images and achieve the interaction between them. The pioneering work of FSS research is proposed by [67], where the support branch directly predicts the weights of the last layer in the query branch for segmentation. Then, the masked average pooling operation is proposed by [68] to extract representative support features, which is widely adopted by subsequent works. More recently, a large number of works [12], [69], [70] build powerful modules on the frozen backbone network to improve the adaptability of the models to unseen categories.

Referring Expression Segmentation (RES) explores object segmentation guided by a textual expression. RES aims to segment visual objects based on the expression, and the two-branch architecture is also adopted by the networks in this research. The first work is introduced by [11], where the visual and linguistic features are first extracted by a visual encoder and a language encoder respectively, and their concatenation is employed to generate the segmentation mask. Subsequently, a series of methods based on multi-level visual features [71], multi-modal LSTM [72], attention mechanism [73], [74], collaborative network [75] are incorporated in RES methods successively to generate more accurate results. In addition, the text descriptions are also adopted by [76] as references for the richness of image content to achieve a better fixation prediction.

In this paper, the proposed Ref-COD also belongs to a referring object segmentation task. However, different from the existing methods, the collection of its referring information does not take much effort. To be specific, it neither needs to collect rare and hard-to-label images containing

target camouflaged objects nor annotates detailed text descriptions for existing COD datasets, which is convenient for academia and industry to follow.

3 PROPOSED DATASET

The emergence of a series of datasets build the basis for carrying out artificial intelligence research, especially in the current data-hunger deep learning era. Besides, the quality of a dataset plays an important role in its lifespan as a benchmark, as stated in [77], [78]. With this in mind, we build a large-scale dataset, named R2C7K, for the proposed Ref-COD task. In this section, we introduce the construction process and statistics of this dataset, respectively.

3.1 Data Collection and Annotations

To construct the R2C7K dataset, the first step is to determine which camouflaged objects to detect. To this end, we investigate the most popular datasets in COD research, *i.e.*, COD10K [1], CAMO [79], and NC4K [80]. Considering that COD10K is the largest and most comprehensively annotated camouflage dataset, we build the Camo-subset of R2C7K mainly based on it. Specifically, we eliminate a few unusual categories, *e.g.* pagurian, crocodile-fish, *etc.*, and attain 4,966 camouflaged images covering 64 categories. For the images containing only one camouflaged object, we directly adopt the annotations provided by COD10K, and for other images containing multiple camouflaged objects, we erase the annotated pixels except for objects of the referring category. Note that we also supplement 49 samples from NC4K for some categories due to their extremely small sample numbers.

Next, we construct the Ref-subset of R2C7K according to the selected 64 categories. We use these category names as keywords and search 25 images that come from real-world scenarios and contain the desired salient objects from the Internet for each category. In particular, these referring images, which have no copyright disputes, are collected from Flickr and Unsplash. For the details on the image collection scheme, we recommend the readers to refer to [81].

Finally, we present the image and annotation samples of the R2C7K dataset in Fig. 2.

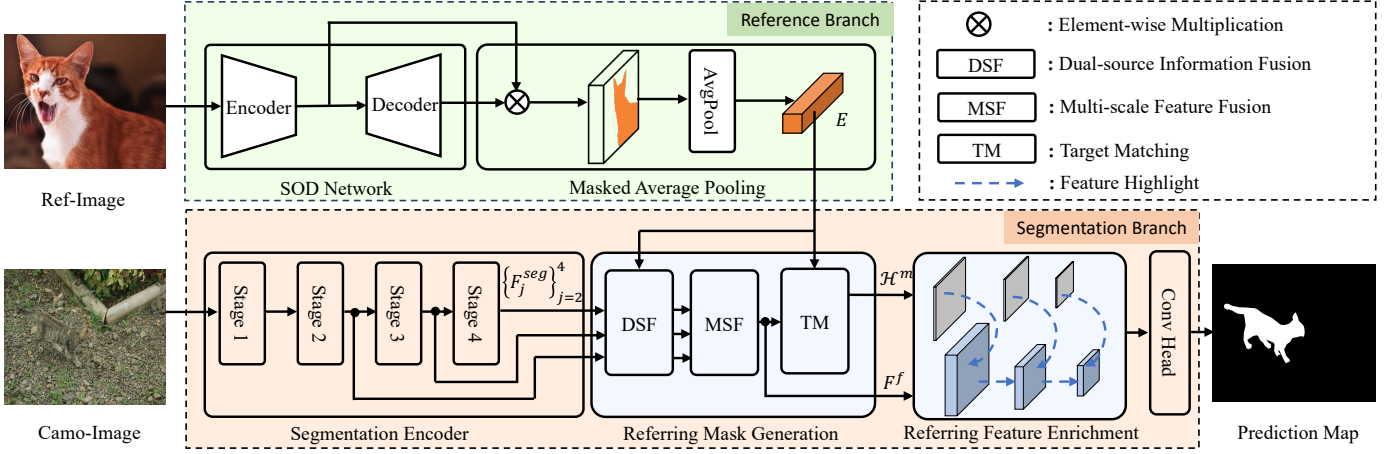


Fig. 6. Overall architecture of our R2CNet framework, which is composed of two branches, *i.e.*, reference branch in green and segmentation branch in orange. In the reference branch, the common representations of a specified object from images is obtained by masking and pooling the visual features with the foreground map generated by a SOD network. In the segmentation branch, the visual features from the last three layers of the encoder are employed to represent the given image. Then, these two kinds of feature representations are fused and compared in the well-designed RMG module to generate a mask prior, which is used to enrich the visual features among different scales to highlight the camouflaged targets in our RFE module. Finally, the enriched features are fed into the decoder to generate the final segmentation map.

objects by matching the targets provided by the references. In particular, the input of a Ref-COD system is composed of two parts, where the first part is an image with camouflaged objects, termed as $I^{camo} \in \mathbb{R}^{3 \times H \times W}$, while the other part is a few referring images with salient target objects, denoted as $I^{ref} = \{I_i^{ref}\}_{i=1}^K, I_i^{ref} \in \mathbb{R}^{3 \times H \times W}$, where H and W denote the height and width of the given images, and K represents the number of referring images. Note that I^{camo} comes from the Camo-subset of R2C7K, and it contains camouflaged objects in a specified category c . Meanwhile, I_i^{ref} is sampled from the Ref-subset, and its salient objects are in category c . The output of Ref-COD is a binary mask M^{seg} for the camouflaged objects of category c in I^{camo} .

4.2 Overall Architecture

Fig. 6 illustrates the overall architecture of our proposed R2CNet. As can be seen, this framework consists of two branches, *i.e.*, the reference branch and the segmentation branch, which will be described in detail.

Reference Branch. The pipeline of extracting common representation from referring images is cascaded by a SOD network based on the encoder-decoder structure and a masked average pooling (MAP) function. In particular, the former is used to generate the visual features and foreground predictions of the referring images, and the latter one is employed to filter out irrelevant information in the referring images. By default, the pre-trained ICON [56] model with ResNet-50 [82] backbone is selected as our SOD network.

Given K referring images with salient target objects and spatial size $H \times W$, the visual features with spatial size $\frac{H}{32} \times \frac{W}{32}$ and foreground maps with spatial size $H \times W$ are first extracted from the encoder and decoder of the SOD network. We denote them as $\{F_k^{ref}\}_{k=1}^K$ and $\{M_k^{ref}\}_{k=1}^K$, respectively. Then, $\{F_k^{ref}\}_{k=1}^K$ and $\{M_k^{ref}\}_{k=1}^K$ are fed into the MAP function to calculate representations associated with the foreground objects, denoted as $F_k^{obj} \in \mathbb{R}^{c_d \times 1 \times 1}$.

This calculation can be formulated as:

$$F_k^{obj} = \mathcal{F}_{conv1 \times 1} \left(\frac{\sum_{2d} (\mathcal{F}_{down}(M_k^{ref}) \otimes F_k^{ref})}{\sum_{2d}(F_k^{ref})} \right), \quad (1)$$

where \otimes is the element-wise multiplication operation, $\mathcal{F}_{down}(\cdot)$ is a bilinear downsampling operation for shape matching, $\sum_{2d}(\cdot)$ accumulates the feature values along the spatial dimension, and $\mathcal{F}_{conv1 \times 1}(\cdot)$ is a 1×1 convolution that transforms the channel of its input to c_d to achieve a better trade-off between efficiency and performance. Finally, we abstract the common representations of target objects in the embedding space, denoted as $E \in \mathbb{R}^{c_d \times 1 \times 1}$, by averaging these object representations.

Segmentation Branch. Our segmentation branch is built upon an encoder-decoder structure as well, which has been widely used in COD research. Note that as the goal of this paper is to provide a new scheme for directionally segmenting the camouflaged objects, we do not put too much effort on the architectural design. In fact, we find that under the proposed scheme, even a simple segmentation network can still perform well. Thus, ResNet-50 [82] is adopted as the encoder, and the features from its last three layers are selected as visual representations, following previous works [1], [3]. The decoder is a convolutional head consisting of two convolutional layers for the identification of camouflaged objects. We also propose two new modules, namely referring mask generation (RMG) and referring feature enrichment (RFE), which are added between the encoder and the decoder, to take advantage of the common representations from the reference branch for the explicit segmentation of camouflaged targets.

Given an image with camouflaged objects and spatial size $H \times W$, we first extract multi-scale features from the last three stages from the encoder. The channels of these features are converted to c_d using 1×1 convolutions. We denote these features as $\{F_j^{seg}\}_{j=2}^4$, where $F_j^{seg} \in \mathbb{R}^{c_d \times \frac{H}{2^{j+1}} \times \frac{W}{2^{j+1}}}$. Then, the resulting features are fed into the RMG module together with the common representations from the reference branch

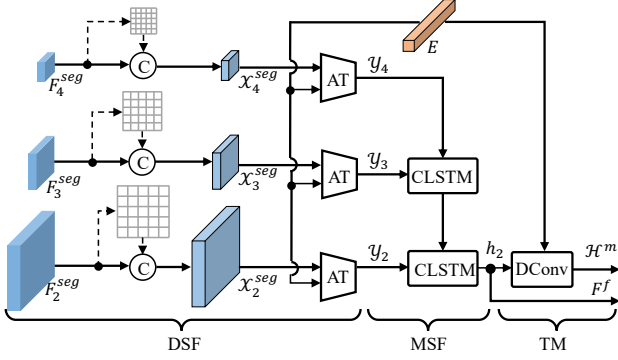


Fig. 7. Structural details of the proposed Referring Mask Generation (RMG) module. Note that ‘C’ is the concatenation operation, ‘AT’ is the affine transformation, ‘CLSTM’ is the convolutional long short-term memory, and ‘Dconv’ is the dynamic convolution.

to generate fusion features and a referring mask, which are denoted as $F^f \in \mathbb{R}^{c_d \times \frac{H}{8} \times \frac{W}{8}}$ and $\mathcal{H}^m \in \mathbb{R}^{1 \times \frac{H}{8} \times \frac{W}{8}}$. This process can be defined as:

$$F^f, \mathcal{H}^m = \text{RMG}(\{F_j^{\text{seg}}\}_{j=2}^4, E). \quad (2)$$

Note that \mathcal{H}^m is a heatmap mask, in which higher scores mean the corresponding positions are more associated with the common representations, and vice versa.

Next, the fusion features are enriched at multiple scales with the guidance of the prior mask to highlight the camouflaged targets in the RFE module, which is defined as:

$$F^{\text{enr}} = \text{RFE}(F^f, \mathcal{H}^m). \quad (3)$$

Finally, the resulting features are fed into the decoder to generate the segmentation map $M^{\text{seg}} \in \mathbb{R}^{1 \times H \times W}$.

4.3 Referring Mask Generation

In order to identify the camouflaged objects accurately from their highly similar surroundings according to the image guidance, a pixel-level comparison between the common representations of target objects and the visual features should be performed. However, the appearance of a camouflaged object may be significantly different from that of the referring objects even if they belong to the same category. In addition, the common representations and the visual features come from different information sources. Such a large information difference may interfere with the comparison process, making the localization process of the camouflaged targets difficult.

Motivated by recent works on multimodal fusion [71], [83], we solve this issue by performing a dual-source information fusion (DSF) between the common representations and the visual features, as illustrated in Fig. 7. To promote the interaction of these two kinds of information, the spatial position information is first injected into the visual features. Specifically, each position of the visual features is concatenated with an 8d embedding vector akin to the implementation of [84]. We denote the visual features equipped with spatial information as $\{x_j^{\text{seg}}\}_{j=2}^4$, where $x_j^{\text{seg}} \in \mathbb{R}^{(c_d+8) \times \frac{H}{2^{j+1}} \times \frac{W}{2^{j+1}}}$. Then, we apply an affine transformation on the visual features under the guidance of the common representations. In particular, two linear layers

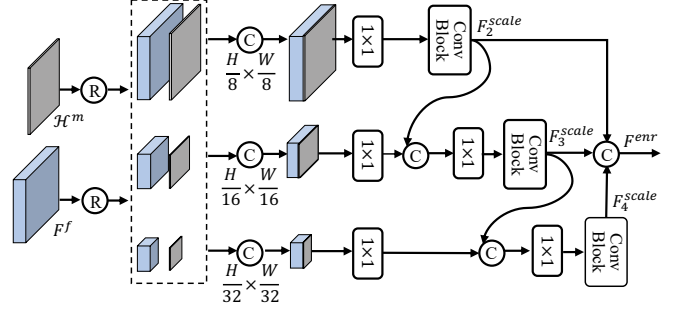


Fig. 8. Structural details of our Referring Feature Enrichment (RFE) module. Note that ‘R’ is the resize operation, ‘ 1×1 ’ is a convolutional layer with kernel size 1, and ‘Conv Block’ is composed of two convolutional layers with kernel size 3.

are utilized to map the common representations to two coefficient vectors, which are applied on the visual features followed by convolution and ReLU operations. The obtained results are denoted as $\{y_j\}_{j=2}^4$, where $y_j \in \mathbb{R}^{c_d \times \frac{H}{2^{j+1}} \times \frac{W}{2^{j+1}}}$. This process is defined as follows:

$$y_j = \mathcal{F}_{\text{relu}}(\mathcal{F}_{\text{conv}3 \times 3}(\mathcal{F}_{\text{relu}}(\gamma_j \otimes x_j^c \oplus \beta_j))), \quad (4)$$

$$\gamma_j = \mathcal{F}_{\text{mlp}1}(E), \beta_j = \mathcal{F}_{\text{mlp}2}(E), \quad (5)$$

where \otimes and \oplus are the element-wise multiplication and addition respectively, $\mathcal{F}_{\text{conv}3 \times 3}(\cdot)$ is a 3×3 convolution for channel recovery, γ_j and β_j are the two coefficient vectors, and $\mathcal{F}_{\text{mlp}1}(\cdot)$ and $\mathcal{F}_{\text{mlp}2}(\cdot)$ denote the two linear layers.

Furthermore, multi-scale fusions (MSF) are performed on the dual-source fusion features along the up-bottom path via convolutional LSTM [85] to enhance the robustness of our method to targets with different scales. This process can be formulated as follows:

$$h_j, c_j = \mathcal{F}_{\text{clstm}}(y_j, [\mathcal{F}_{\text{up}}(h_{j+1}), \mathcal{F}_{\text{up}}(c_{j+1})]), \quad (6)$$

where $\mathcal{F}_{\text{up}}(\cdot)$ is a bilinear upsampling operation for shape matching and $\mathcal{F}_{\text{clstm}}$ denotes a cell of convolutional LSTM. Note that the initial state $h_4 = c_4 = y_4$, and the last hidden state, i.e., $h_2 \in \mathbb{R}^{c_d \times \frac{H}{8} \times \frac{W}{8}}$, is used as the fused feature F^f .

Finally, the common representations are compared with the representations of each position of the fusion features to produce a referring mask, namely \mathcal{H}^m . Inspired by [88], [89], this target-matching (TM) process is realized through a dynamic convolution operation. In particular, the common representations and the fusion features are utilized as reference-guided dynamic kernel and input, respectively.

4.4 Referring Feature Enrichment

Given the referring mask generated above, we design a Referring Feature Enrichment (RFE) module to enrich the visual features at different scales, as shown in Fig 8.

To be specific, the prior mask and the fusion features are first resized to the shapes of the aforementioned three features, i.e., $\{\frac{H}{2^{j+1}} \times \frac{W}{2^{j+1}}\}_{j=2}^4$, respectively. Then, the resized masks and features at the same scale are fused by concatenation, and the output features of different scales, termed as $\{F_j^{\text{scale}}\}_{j=2}^4$, where $F_j^{\text{scale}} \in \mathbb{R}^{c_d \times \frac{H}{2^{j+1}} \times \frac{W}{2^{j+1}}}$, are also concatenated together to enrich the capability of identifying camouflaged objects. We denote the enriched feature as

TABLE 1

Comparison of the COD models with their Ref-COD counterparts. All models are evaluated on a NVIDIA RTX 3090 GPU. ‘R-50’: ResNet-50 [82], ‘E-B4’: EfficientNet-B4 [86], ‘R2-50’: Res2Net-50 [87], ‘R³-50’: Triple ResNet-50 [2]. ‘-Ref’: the model with image references composed of salient objects. ‘Attribute’: the attribute of each network, ‘Single-obj’: the scene of a single camouflaged object, ‘Multi-obj’: the scene of multiple camouflaged objects, ‘Overall’: all scenes containing camouflaged objects. ‘↑’: the higher the better, ‘↓’: the lower the better.

Models	Attribute				Overall				Single-obj				Multi-obj			
	Backbone	Params (M)	Macs (G)	Speed (FPS)	$S_m \uparrow$	$\alpha E \uparrow$	$wF \uparrow$	$M \downarrow$	$S_m \uparrow$	$\alpha E \uparrow$	$wF \uparrow$	$M \downarrow$	$S_m \uparrow$	$\alpha E \uparrow$	$wF \uparrow$	$M \downarrow$
Baseline	R-50	25.97	21.02	185.74	0.772	0.847	0.604	0.044	0.777	0.847	0.611	0.043	0.711	0.849	0.531	0.054
R2CNet	R-50	27.15	23.23	151.47	0.805	0.879	0.669	0.036	0.810	0.880	0.674	0.035	0.747	0.872	0.602	0.046
PFNet ₂₀₂₁ [31]	R-50	48.55	52.99	80.33	0.791	0.876	0.651	0.040	0.795	0.876	0.656	0.039	0.74	0.868	0.594	0.051
PFNet-Ref	R-50	57.58	59.59	72.48	0.811	0.885	0.687	0.036	0.815	0.886	0.691	0.035	0.764	0.873	0.632	0.045
PreyNet ₂₀₂₂ [24]	R-50	38.53	116.01	59.78	0.806	0.890	0.690	0.034	0.811	0.892	0.696	0.033	0.749	0.878	0.618	0.042
PreyNet-Ref	R-50	38.70	117.60	57.04	0.817	0.900	0.704	0.032	0.822	0.900	0.709	0.032	0.763	0.898	0.645	0.041
SINetV2 ₂₀₂₂ [1]	R2-50	26.98	24.48	98.12	0.813	0.874	0.678	0.036	0.818	0.874	0.684	0.035	0.763	0.864	0.615	0.045
SINetV2-Ref	R2-50	27.70	26.01	86.60	0.823	0.888	0.700	0.033	0.828	0.889	0.705	0.032	0.771	0.874	0.634	0.043
BSANet ₂₀₂₂ [37]	R2-50	32.59	59.29	71.75	0.818	0.893	0.702	0.034	0.823	0.895	0.707	0.033	0.766	0.873	0.643	0.041
BSANet-Ref	R2-50	33.07	66.08	67.18	0.830	0.912	0.727	0.030	0.827	0.913	0.733	0.030	0.774	0.895	0.655	0.039
BGNet ₂₀₂₂ [4]	R2-50	79.85	116.76	66.29	0.818	0.901	0.679	0.036	0.822	0.901	0.683	0.035	0.775	0.886	0.626	0.044
BGNet-Ref	R2-50	151.06	171.03	50.69	0.840	0.909	0.738	0.029	0.844	0.910	0.742	0.029	0.792	0.887	0.679	0.036
ZoomNet ₂₀₂₂ [2]	R ³ -50	32.38	203.50	22.89	0.813	0.884	0.688	0.032	0.818	0.885	0.695	0.031	0.747	0.870	0.605	0.042
ZoomNet-Ref	R ³ -50	33.30	218.24	20.82	0.834	0.886	0.720	0.029	0.839	0.887	0.726	0.029	0.781	0.876	0.652	0.038
DGNet ₂₀₂₃ [3]	E-B4	19.22	5.53	110.57	0.816	0.883	0.684	0.034	0.826	0.885	0.700	0.032	0.744	0.873	0.588	0.047
DGNet-Ref	E-B4	20.10	7.24	95.06	0.821	0.891	0.696	0.032	0.827	0.890	0.703	0.031	0.748	0.879	0.607	0.045

$F^{enr} \in \mathbb{R}^{c_d \times \frac{H}{8} \times \frac{W}{8}}$. As mentioned in PFNet [69], tiny objects may become unclear in the down-sampled feature maps. Thus, we build a similar path that crosses scales from the finer feature to the coarse one to achieve the interaction between them. In addition, we also apply supervision on $\{F_j^{scale}\}_{j=2}^4$ to make the yielded feature F^{enr} more robust, and the corresponding maps is denoted as $\{M_j^{scale}\}_{j=2}^4$ where $M_j^{scale} \in \mathbb{R}^{1 \times H \times W}$.

5 EXPERIMENTS

In this section, we first introduce the experiment settings of this paper, *i.e.*, training & testing protocols, hyperparameter details, and evaluation metrics. Then, we conduct quantitative comparisons between the Ref-COD methods and the corresponding COD methods. Particularly, we compare the proposed R2CNet with the baseline model on different camouflaged scenes. we also apply the design of Ref-COD on 7 recent state-of-the-art COD methods to verify its generality. Next, we report ablative study results to investigate the effectiveness of each component and our design choice. Finally, we carry out visualization comparisons to gain more intuitive insight into our Ref-COD.

5.1 Experiment Setup

Training & Testing Protocols. Considering that the goal of Ref-COD is to generate a binary foreground map closing to the annotation, the structure loss [90] consisting of BCE loss and IoU loss, which has been widely used in many binary segmentation tasks, can be adopted as the optimization objectives of the Ref-COD models. Specifically, this function can be formulated as:

$$\mathcal{L}(P, G) = \sum_{i=1}^4 \mathcal{L}_{bce}(P_i, G) + \mathcal{L}_{iou}(P_i, G), \quad (7)$$

where $P = \{M_2^{scale}, M_3^{scale}, M_4^{scale}, M^{seg}\}$ represent the predictions generated by our model, and G refers to the ground truth annotation.

Hyperparameter Details. By default, the number of referring images in our Ref-COD is set to 5. During the training stage, the parameters of the foreground prediction network are frozen, the batch size is set to 32, the optimizer we adopt is Adam [91], and the learning rate is initialized to 5e-4 and gradually decays according to the cosine annealing method [92]. During inference, all images are first resized to 352×352 and then fed into the trained R2CNet to generate the final prediction without any post-processing operations. All experiments are implemented in PyTorch [93].

Metrics. Following the standard protocol in COD, we adopt four common metrics for evaluation, including mean absolute error (M) [14], structure-measure (S_m) [15], adaptive E-measure (αE) [16] and weighted F-measure (wF) [17]. To be specific, M measures the absolute difference between the predicted mask and ground-truth (GT); S_m measures the region-aware and object-aware structural similarity between the predicted map and GT; αE measures the element-wise and image-level similarity. wF is an exhaustive measure of both recall and precision between the prediction and GT. In addition, we draw the precision-recall (PR) curves and F_β -threshold (F_β) curves for further comparison.

5.2 Quantitative Evaluation

Comparison with Baselines. To verify the effectiveness of our R2CNet, we first compare it with its baseline variant, which is a standard COD model based on encoder-decoder architecture. In this baseline model, the last three features from its encoder are fused along the up-bottom path, following the fashion in FPN, and the fused feature is fed to its decoder to directly segment camouflaged objects without any reference. As shown in Tab. 1, our R2CNet surpasses

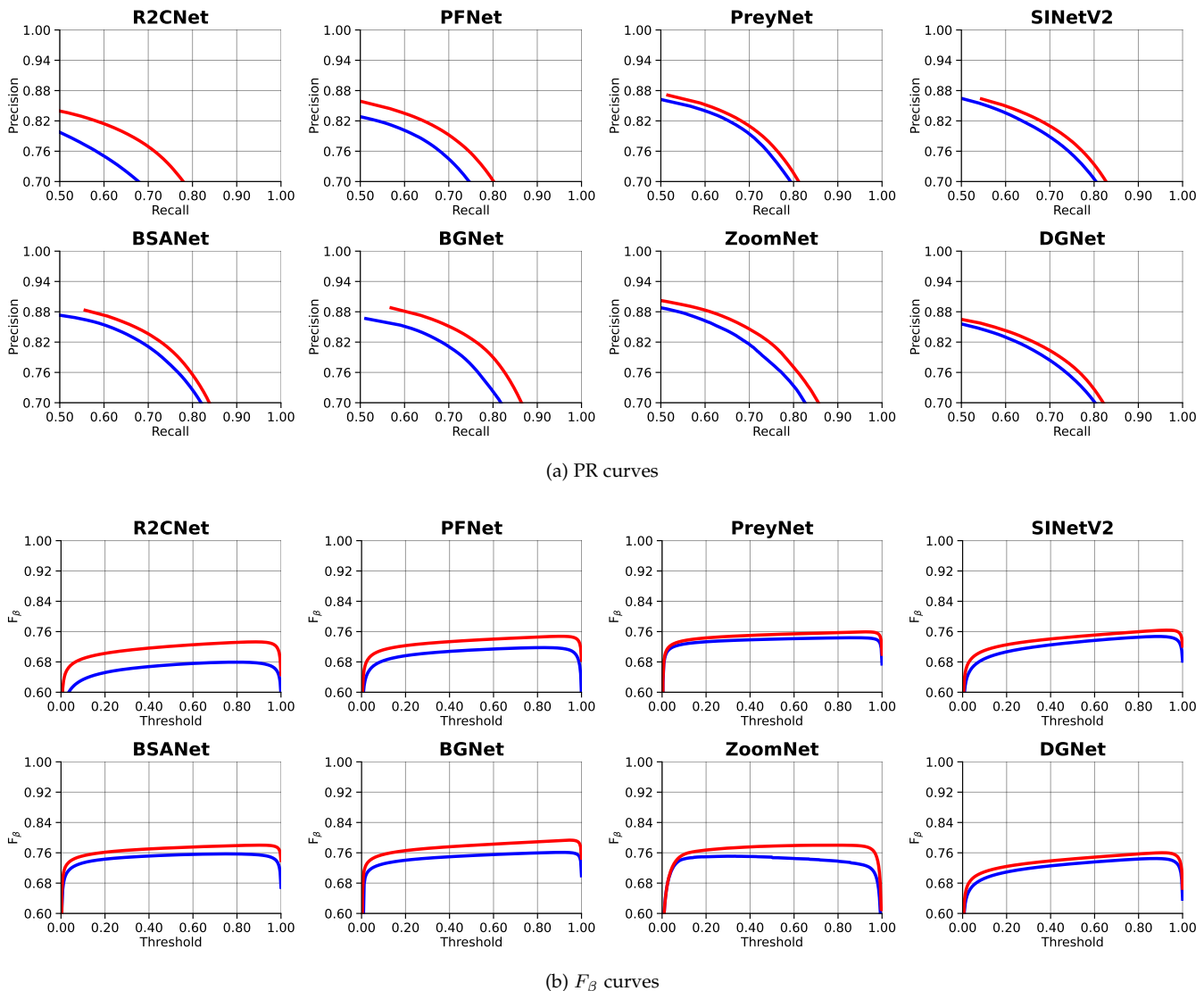


Fig. 9. PR and F_β curves of the COD methods and their Ref-COD variants. The results of standard COD methods and their Ref-COD counterparts are shown via blue and red solid lines respectively.

the baseline model by a large margin across all metrics in the overall scene (*i.e.*, test split) of R2C7K. To evaluate the performance of the model more comprehensively, we further divide the overall scene into two groups, namely the scene of single camouflaged objects and the scene of multiple camouflaged objects. It can be observed that our R2CNet still outperforms its COD baseline in all settings, which demonstrates that the referring images contribute to the identification of the camouflaged objects from the confusing scenes.

Application to Existing COD Methods. To verify the generality of our Ref-COD design, we also apply this idea to existing COD methods. These methods are chosen according to three criteria: a) recently published, b) representative, and c) with open source code. In particular, the methods to participate in the adaptation here include: PFNet [31], PreyNet [24], SINetV2 [1], BSANet [37], BGNet [4], ZoomNet [2], and DGNet [3]. As shown in the third to last row of Tab. 1 and Fig. 9, the Ref-COD variants of these models achieve better performance than their original versions

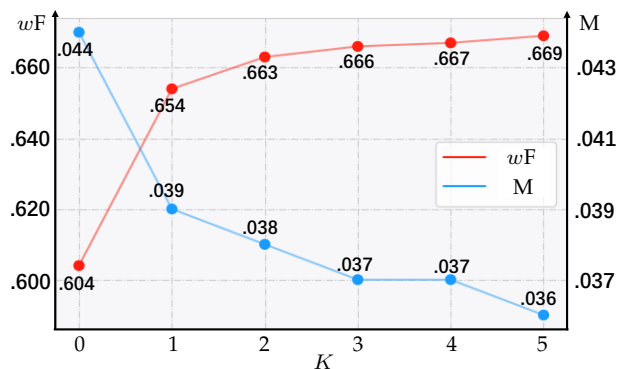


Fig. 10. Ablation experiments on the number of referring images.

across all metrics. It is noteworthy that our lightweight baseline model even achieves comparable performance to recent COD methods after incorporating referring images. This indicates that our method does not rely on powerful segmentation networks. The introduction of the reference branch can help significantly improve the performance of

TABLE 2

Ablation experiments on the components of our R2CNet. RMG: the Referring Mask Generation Module. RFE: the Referring Feature Enhance Module.

No.	RMG	RFE	$S_m \uparrow$	$\alpha E \uparrow$	$wF \uparrow$	$M \downarrow$
1			0.772	0.847	0.604	0.044
2	✓		0.800	0.870	0.661	0.038
3		✓	0.792	0.869	0.644	0.040
4	✓	✓	0.805	0.879	0.669	0.036

TABLE 3

Ablation experiments on the fusion strategies in the RMG module. ‘DSF’: the fusion between the common representations and visual features; ‘MSF’: the fusion of features at different scales. ‘ $\mathcal{F}_{multiply}$ ’: element-wise multiplication. ‘ $\mathcal{F}_{at}(\cdot)$ ’: affine transformation. ‘ \mathcal{F}_{concat} ’: concatenation. ‘ $\mathcal{F}_{clstm}(\cdot)$ ’: convolutional lstmcell.

No.	DSF	MSF	$S_m \uparrow$	$\alpha E \uparrow$	$wF \uparrow$	$M \downarrow$
1	$\mathcal{F}_{multiply}$	\mathcal{F}_{concat}	0.801	0.870	0.656	0.039
2	$\mathcal{F}_{multiply}$	\mathcal{F}_{clstm}	0.802	0.872	0.659	0.038
3	\mathcal{F}_{at}	\mathcal{F}_{concat}	0.804	0.872	0.666	0.037
4	\mathcal{F}_{at}	\mathcal{F}_{clstm}	0.805	0.879	0.669	0.036

a COD model even though it is not strong, reflecting the effectiveness of our Ref-COD idea.

5.3 Ablative Studies

Number of referring images. We ablate the number of referring images, *i.e.* K , for its impact on the Ref-COD. Considering that there are 5 referring images in each category of the test split of the R2C7K dataset, the value of K changes from 0 to 5. When ‘ $0 < K < 5$ ’, the performance of our R2CNet is calculated by averaging three evaluations, in which this model is guided by K referring images randomly sampled from a certain category of the test split. The experimental results in Fig. 10 show that the performance of our R2CNet improves with the increase of the number of referring images. We believe this is because the acquired common information is less affected by sample differences during this process, and thus a more accurate location of camouflaged targets is achieved.

Model Components. We analyze the importance of each component in our R2CNet, and the experimental results are shown in Tab. 2. It can be observed that both of our modules can boost the performance of our model, where the RMG module improves the wF score from 0.604 to 0.661 and the RFE module improves this score from 0.604 to 0.644. And a more outstanding performance improvement (from 0.604 to 0.669, *i.e.*, 10.8%) appears when we combine them together. These results confirm the effectiveness of the two modules in segmenting camouflaged objects according to the referring images.

Ablation on RMG module. We provide two variants for both the cross-source fusion and the cross-scale fusion of the referring representations and visual features in our RMG module. As shown in Tab. 3, our chosen strategy achieves the best performance among the four combinations.

Ablation on RFE module. We investigate four feasible strategies for feature enrichment in our module. These

TABLE 4

Ablation experiments on the feature enrichment strategy in the RFE module. ‘w/o CSP’ or ‘w/ CSP’: multi-scale enrichment without or with the cross-scale path.

No.	Setting	Speed (FPS)	$S_m \uparrow$	$\alpha E \uparrow$	$wF \uparrow$	$M \downarrow$
1	ASPP [94]	143.07	0.803	0.871	0.663	0.038
2	RFB [95]	144.03	0.801	0.872	0.662	0.038
3	w/o CSP	134.13	0.803	0.873	0.665	0.037
4	w/ CSP	130.95	0.805	0.879	0.669	0.036

TABLE 5

Ablation experiments on the channel number of our R2CNet.

No.	Setting	Macs (G)	Params (M)	$S_m \uparrow$	$\alpha E \uparrow$	$wF \uparrow$	$M \downarrow$
1	$c_d = 32$	10.6	24.0	0.799	0.871	0.655	0.039
2	$c_d = 64$	11.7	25.0	0.805	0.879	0.669	0.036
3	$c_d = 128$	15.8	29.1	0.807	0.875	0.672	0.037
4	$c_d = 256$	32.2	44.4	0.811	0.884	0.679	0.036

methods include two plug-and-play fashions and two variants of our multi-scale enrichment manner. As can be observed in Tab. 4, our well-designed strategies achieve better performance under reasonable inference speed, especially the one with the cross-scale path.

Model Dimension. The dimension of the model (c_d) has a significant impact on its parameter scale and inference speed, and we thus conduct several experiments to select a suitable dimension value. Specifically, we increase c_d from 32 to 256 in a doubling fashion, and the changes in model parameters, computational cost, and performance during this process are shown in Tab. 5. It can be observed that the performance of our R2CNet continues to improve during the increase of c_d . However, when c_d is greater than 64, the improvement of performance begins to decrease, while the parameters and calculation cost of the model increase sharply. For example, when c_d increases from 64 to 128, the performance of our R2CNet improves slightly, but the computational overhead increases by 35% (No.2 *vs.* No.3). Therefore, we set c_d to 64 for the trade-off between the performance and the efficiency of our R2CNet.

Reference Forms. We also investigate three different forms of reference information, *i.e.*, text descriptions, images with camouflaged objects, and images with salient objects. As discussed in Sec. 1 and Sec. 2, it is difficult to obtain the detailed text descriptions and the annotated images containing the camouflaged objects associated with the camouflaged targets in the given images. Here we consider the readily available versions of text descriptions and images with camouflaged objects, and compare their upper bounds with our chosen reference, *i.e.*, images with salient objects.

For text reference, inspired by recent prompt engineering, we first build text descriptions with ‘a photo of [CLASS]’, where ‘[CLASS]’ denotes one of the 64 categories in our R2C7K. Then, we feed these 64 text descriptions into the pre-trained CLIP [96] that adopts ResNet-50 as visual backbone, to get the textual features, following CLIPSeg [97]. These features are used as the common representations of target objects. Note that we adopt the same text representations for the samples belonging to the same

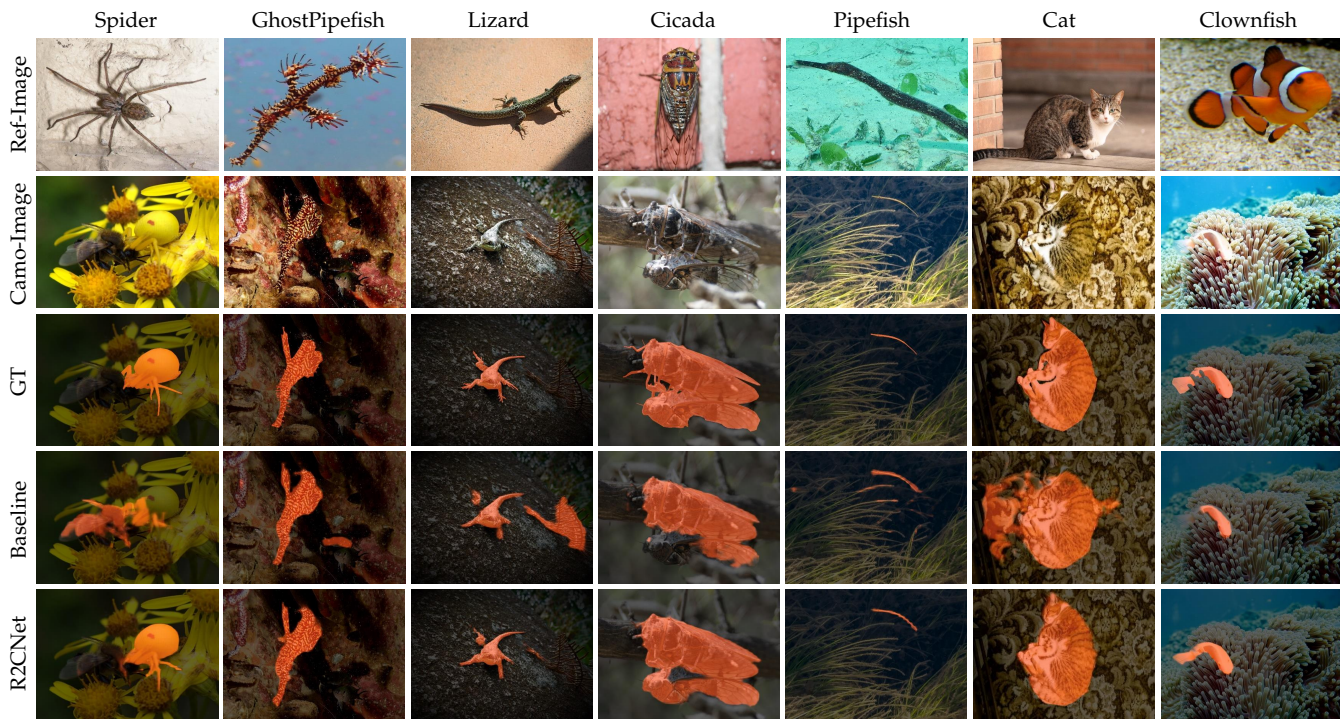


Fig. 11. Visual comparisons of the predictions between the proposed Ref-COD method (R2CNet) and the standard COD method (Baseline). The segmentation masks are shown in purple.

TABLE 6

Ablation experiments on the form of Ref-COD. text-ref: text with a simple prompt; camo-ref: image with camouflaged objects; sal-ref: image with salient objects; LSM: using large-scale pre-trained model; GT: using GT mask of the reference; Seen: the reference representations used in training appears in testing.

No.	Methods	LSM	GT	Seen	$S_m \uparrow$	$\alpha E \uparrow$	$wF \uparrow$	$M \downarrow$
1	Baseline				0.772	0.847	0.604	0.044
2	+ text-ref	✓		✓	0.805	0.872	0.661	0.038
3	+ camo-ref		✓		0.801	0.869	0.656	0.039
4	+ sal-ref				0.805	0.879	0.669	0.036

category in the training set and testing set.

For image reference with camouflaged objects, we first randomly sample several images from the Camo-subset of the category to which the target objects belong. Then, we send them into ResNet-50 to extract visual features. Note that these features are masked and pooled with ground-truth annotations to get the common representations.

The experimental results are shown in Tab. 6. Note that the text reference employs a large-scale pre-trained model and the common representations in testing have been seen during training. The camouflage candidate adopts GT annotations as masks to capture the common representations. Despite these, our R2CNet using salient object reference still achieves better performance than them. These experiments indicate that referring images with salient objects can more effectively discover and segment the camouflaged objects.

5.4 Qualitative Evaluation

Results Visualization. We first present the visual comparison of prediction results of our referring COD method, *i.e.*, R2CNet, and the class-agnostic COD method, *i.e.*, Baseline, in

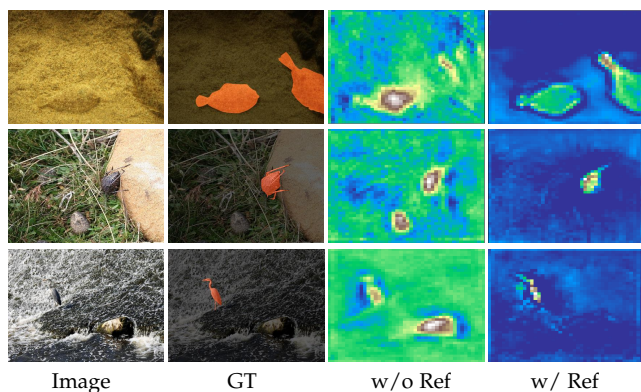


Fig. 12. Visual comparison of the intermediate features between the methods with or without reference.

Fig. 11. As shown in these scenes from the 1st (Spider) to the 4th column (Cicada), there are multiple camouflaged objects. The baseline model tends to indiscriminately segment all potential camouflaged objects, and thus its outputs are often inaccurate. To be specific, it may not only miss some camouflaged objects (*e.g.*, Cicada), but also mispredict other objects as camouflaged ones (*e.g.*, Spider and Lizard). For all these challenging scenes, our R2CNet is able to identify the camouflaged objects orienting to referring images. In addition, compared with the baseline model, our R2CNet is less disturbed by other similar objects (*e.g.*, Pipefish). And it can segment visual objects more completely in scenes with only one camouflaged object but with less difference from the surrounding, as shown in the 6th column (Cat) and 7th column (Clownfish). We argue that this is because the common representations of a certain category of objects learned from the referring images are conducive to identifying the main body of such camouflaged objects.

Features Visualization. To gain more insights from the Ref-COD, we also visualize intermediate features with or without referring information, as shown in Fig. 12. As can be seen, the model without references can locate the camouflaged objects but it may be disturbed by other objects, and produces inaccurate segmentation results. With the incorporation of references, the model can focus more on the indicated camouflaged objects, regardless of other ones.

6 FUTURE WORK

Based on the R2C7K dataset and R2CNet framework proposed in this paper, there are a few foreseeable directions about the Ref-COD to explore in future research:

1) Other Forms of References. In recent years, multi-modal research has made great progress in vision and language, vision and speech, *etc.* Based on them, it is interesting to explore Ref-COD with other references, *e.g.*, text and speech. As discussed above, the main challenge depends on how to obtain these references easily and efficiently.

2) Special Case of Referring Scene. In this paper, we assume the image to be segmented contains the target objects specified by the referring images. However, such objects may not exist in some real scenes. It will be promising to extend Ref-COD to be compatible with these cases.

3) Related Tasks. In some application scenarios, users only need some simple answers to make decisions, rather than using more complex equipment to obtain the segmentation details of camouflaged objects. Therefore, it is also valuable to extend the Ref-COD to simple tasks related to question answering.

7 CONCLUSIONS

We propose a novel benchmark named Ref-COD to directionally segment the camouflaged object with simple image references. First, we build a large-scale dataset (*i.e.*, R2C7K) consisting of images in real-world scenarios. Then, we develop an end-to-end Reference to COD framework (*i.e.*, R2CNet), which follows the two-branch architecture. Particularly, the introduction of our well-designed RMG module and RFE module facilitates the guidance of the common representations from referring images to the challenging segmentation of camouflaged objects. Compared with the COD counterpart which indiscriminately segments camouflaged objects from the background, our R2CNet achieves significantly superior performance on the common metrics, and generates more visually favorable predictions. We believe it is promising to establish a multi-information collaborative system, and we hope the perspective provided by our Ref-COD will inspire future work.

REFERENCES

- [1] D.-P. Fan, G.-P. Ji, M.-M. Cheng, and L. Shao, "Concealed object detection," *IEEE TPAMI*, vol. 44, no. 10, pp. 6024–6042, 2022.
- [2] Y. Pang, X. Zhao, T.-Z. Xiang, L. Zhang, and H. Lu, "Zoom in and out: A mixed-scale triplet network for camouflaged object detection," in *IEEE CVPR*, 2022.
- [3] G.-P. Ji, D.-P. Fan, Y.-C. Chou, D. Dai, A. Liniger, and L. Van Gool, "Deep gradient learning for efficient camouflaged object detection," *MIR*, vol. 20, no. 1, pp. 92–108, 2023.
- [4] Y. Sun, S. Wang, C. Chen, and T.-Z. Xiang, "Boundary-guided camouflaged object detection," in *IJCAI*, 2022.
- [5] D.-P. Fan, G.-P. Ji, T. Zhou, G. Chen, H. Fu, J. Shen, and L. Shao, "Pranet: Parallel reverse attention network for polyp segmentation," in *MICCAI*, 2020.
- [6] D.-P. Fan, T. Zhou, G.-P. Ji, Y. Zhou, G. Chen, H. Fu, J. Shen, and L. Shao, "Inf-net: Automatic covid-19 lung infection segmentation from ct images," *IEEE TMI*, vol. 39, no. 8, pp. 2626–2637, 2020.
- [7] D. Tabernik, S. Šela, J. Skvarč, and D. Škočaj, "Segmentation-based deep-learning approach for surface-defect detection," *J. Intell. Manuf.*, vol. 31, no. 3, pp. 759–776, 2020.
- [8] X. Le, J. Mei, H. Zhang, B. Zhou, and J. Xi, "A learning-based approach for surface defect detection using small image datasets," *Neurocomputing*, 2020.
- [9] M. Türkoğlu and D. Hanbay, "Plant disease and pest detection using deep learning-based features," *Turk J Elec Eng & Comp Sci*, vol. 27, no. 3, pp. 1636–1651, 2019.
- [10] T. Troscianko, C. P. Benton, P. G. Lovell, D. J. Tolhurst, and Z. Pizlo, "Camouflage and visual perception," *Philos. Trans. R. Soc. B: Biol. Sci.*, vol. 364, no. 1516, pp. 449–461, 2009.
- [11] R. Hu, M. Rohrbach, and T. Darrell, "Segmentation from natural language expressions," in *ECCV*, 2016.
- [12] C. Zhang, G. Lin, F. Liu, R. Yao, and C. Shen, "Canet: Class-agnostic segmentation networks with iterative refinement and attentive few-shot learning," in *IEEE CVPR*, 2019.
- [13] T.-Y. Lin, P. Dollár, R. Girshick, K. He, B. Hariharan, and S. Belongie, "Feature pyramid networks for object detection," in *IEEE CVPR*, 2017.
- [14] F. Perazzi, P. Krähenbühl, Y. Pritch, and A. Hornung, "Saliency filters: Contrast based filtering for salient region detection," in *IEEE CVPR*, 2012.
- [15] D.-P. Fan, M.-M. Cheng, Y. Liu, T. Li, and A. Borji, "Structure-measure: A new way to evaluate foreground maps," in *IEEE ICCV*, 2017.
- [16] D.-P. Fan, C. Gong, Y. Cao, B. Ren, M.-M. Cheng, and A. Borji, "Enhanced-alignment measure for binary foreground map evaluation," in *IJCAI*, 2018.
- [17] R. Margolin, L. Zelnik-Manor, and A. Tal, "How to evaluate foreground maps?" in *IEEE CVPR*, 2014.
- [18] D.-P. Fan, G.-P. Ji, G. Sun, M.-M. Cheng, J. Shen, and L. Shao, "Camouflaged object detection," in *IEEE CVPR*, 2020.
- [19] Y. Sun, G. Chen, T. Zhou, Y. Zhang, and N. Liu, "Context-aware cross-level fusion network for camouflaged object detection," *arXiv preprint arXiv:2105.12555*, 2021.
- [20] M.-C. Chou, H.-J. Chen, and H.-H. Shuai, "Finding the achilles heel: Progressive identification network for camouflaged object detection," in *IEEE ICME*, 2022.
- [21] M. Zhuge, X. Lu, Y. Guo, Z. Cai, and S. Chen, "Cubenet: X-shape connection for camouflaged object detection," *PR*, vol. 127, p. 108644, 2022.
- [22] G. Chen, S.-J. Liu, Y.-J. Sun, G.-P. Ji, Y.-F. Wu, and T. Zhou, "Camouflaged object detection via context-aware cross-level fusion," *IEEE TCSVT*, vol. 32, no. 10, pp. 6981–6993, 2022.
- [23] Q. Jia, S. Yao, Y. Liu, X. Fan, R. Liu, and Z. Luo, "Segment, magnify and reiterate: Detecting camouflaged objects the hard way," in *IEEE CVPR*, 2022.
- [24] M. Zhang, S. Xu, Y. Piao, D. Shi, S. Lin, and H. Lu, "Preynet: Preying on camouflaged objects," in *ACM MM*, 2022.
- [25] K. Wang, H. Bi, Y. Zhang, C. Zhang, Z. Liu, and S. Zheng, "D² c-net: A dual-branch, dual-guidance and cross-refine network for camouflaged object detection," *IEEE TIE*, vol. 69, no. 5, pp. 5364–5374, 2021.
- [26] Q. Zhai, X. Li, F. Yang, C. Chen, H. Cheng, and D.-P. Fan, "Mutual graph learning for camouflaged object detection," in *IEEE CVPR*, 2021.
- [27] R. He, Q. Dong, J. Lin, and R. W. Lau, "Weakly-supervised camouflaged object detection with scribble annotations," in *AAAI*, 2022.
- [28] A. Li, J. Zhang, Y. Lv, B. Liu, T. Zhang, and Y. Dai, "Uncertainty-aware joint salient object and camouflaged object detection," in *IEEE CVPR*, 2021.
- [29] J. Liu, J. Zhang, and N. Barnes, "Modeling aleatoric uncertainty for camouflaged object detection," in *IEEE WACV*, 2022.
- [30] N. Kajiura, H. Liu, and S. Satoh, "Improving camouflaged object detection with the uncertainty of pseudo-edge labels," in *ACM MM Asia*, 2021.
- [31] H. Mei, G.-P. Ji, Z. Wei, X. Yang, X. Wei, and D.-P. Fan, "Camouflaged object segmentation with distraction mining," in *IEEE CVPR*, 2021.

- [32] B. Yin, X. Zhang, Q. Hou, B.-Y. Sun, D.-P. Fan, and L. Van Gool, "Camoformer: Masked separable attention for camouflaged object detection," *arXiv preprint arXiv:2212.06570*, 2022.
- [33] W. Zhai, Y. Cao, H. Xie, and Z.-J. Zha, "Deep texton-coherence network for camouflaged object detection," *IEEE TMM*, 2022.
- [34] C. Zhang, K. Wang, H. Bi, Z. Liu, and L. Yang, "Camouflaged object detection via neighbor connection and hierarchical information transfer," *CVIU*, vol. 221, p. 103450, 2022.
- [35] Y. Cheng, H.-Z. Hao, Y. Ji, Y. Li, and C.-P. Liu, "Attention-based neighbor selective aggregation network for camouflaged object detection," in *IEEE IJCNN*, 2022, pp. 1–8.
- [36] D.-P. Fan, G.-P. Ji, P. Xu, M.-M. Cheng, C. Sakaridis, and L. Van Gool, "Advances in deep concealed scene understanding," *VINT*, 2023.
- [37] H. Zhu, P. Li, H. Xie, X. Yan, D. Liang, D. Chen, M. Wei, and J. Qin, "I can find you! boundary-guided separated attention network for camouflaged object detection," in *AAAI*, 2022.
- [38] T. Zhou, Y. Zhou, C. Gong, J. Yang, and Y. Zhang, "Feature aggregation and propagation network for camouflaged object detection," *IEEE TIP*, vol. 31, pp. 7036–7047, 2022.
- [39] X. Qin, D.-P. Fan, C. Huang, C. Diagne, Z. Zhang, A. C. Sant'Anna, A. Suarez, M. Jagersand, and L. Shao, "Boundary-aware segmentation network for mobile and web applications," *arXiv preprint arXiv:2101.04704*, 2021.
- [40] G.-P. Ji, L. Zhu, M. Zhuge, and K. Fu, "Fast camouflaged object detection via edge-based reversible re-calibration network," *PR*, vol. 123, p. 108414, 2022.
- [41] J. Zhu, X. Zhang, S. Zhang, and J. Liu, "Inferring camouflaged objects by texture-aware interactive guidance network," in *AAAI*, 2021.
- [42] J. Ren, X. Hu, L. Zhu, X. Xu, Y. Xu, W. Wang, Z. Deng, and P.-A. Heng, "Deep texture-aware features for camouflaged object detection," *IEEE TCSVT*, 2021.
- [43] Y. Zhong, B. Li, L. Tang, S. Kuang, S. Wu, and S. Ding, "Detecting camouflaged object in frequency domain," in *IEEE CVPR*, 2022.
- [44] J. Lin, X. Tan, K. Xu, L. Ma, and R. W. Lau, "Frequency-aware camouflaged object detection," *ACM TMCCA*, vol. 19, no. 2, pp. 1–16, 2023.
- [45] J. Zhang, Y. Lv, M. Xiang, A. Li, Y. Dai, and Y. Zhong, "Depth-guided camouflaged object detection," *arXiv preprint arXiv:2106.13217*, 2021.
- [46] M. Xiang, J. Zhang, Y. Lv, A. Li, Y. Zhong, and Y. Dai, "Exploring depth contribution for camouflaged object detection," *arXiv e-prints*, pp. arXiv–2106, 2021.
- [47] Z. Wu, D. P. Paudel, D.-P. Fan, J. Wang, S. Wang, C. Démonceaux, R. Timofte, and L. Van Gool, "Source-free depth for object pop-out," *arXiv preprint arXiv:2212.05370*, 2022.
- [48] M.-M. Cheng, N. J. Mitra, X. Huang, P. H. Torr, and S.-M. Hu, "Global contrast based salient region detection," *IEEE TPAMI*, vol. 37, no. 3, pp. 569–582, 2014.
- [49] L. Wang, H. Lu, X. Ruan, and M.-H. Yang, "Deep networks for saliency detection via local estimation and global search," in *IEEE CVPR*, 2015.
- [50] J. Kim and V. Pavlovic, "A shape-based approach for salient object detection using deep learning," in *ECCV*, 2016.
- [51] S. He, R. W. Lau, W. Liu, Z. Huang, and Q. Yang, "Supercnn: A superpixelwise convolutional neural network for salient object detection," *IJCV*, vol. 115, pp. 330–344, 2015.
- [52] J. Long, E. Shelhamer, and T. Darrell, "Fully convolutional networks for semantic segmentation," in *IEEE CVPR*, 2015.
- [53] A. Vaswani, N. Shazeer, N. Parmar, J. Uszkoreit, L. Jones, A. N. Gomez, Ł. Kaiser, and I. Polosukhin, "Attention is all you need," in *NeurIPS*, 2017.
- [54] X. Zhang, X. Sun, Y. Luo, J. Ji, Y. Zhou, Y. Wu, F. Huang, and R. Ji, "Rstnet: Captioning with adaptive attention on visual and non-visual words," in *IEEE CVPR*, 2021.
- [55] M. Wu, X. Zhang, X. Sun, Y. Zhou, C. Chen, J. Gu, X. Sun, and R. Ji, "Difnet: Boosting visual information flow for image captioning," in *IEEE CVPR*, 2022.
- [56] M. Zhuge, D.-P. Fan, N. Liu, D. Zhang, D. Xu, and L. Shao, "Salient object detection via integrity learning," *IEEE TPAMI*, vol. 45, no. 3, pp. 3738–3752, 2023.
- [57] O. Ronneberger, P. Fischer, and T. Brox, "U-net: Convolutional networks for biomedical image segmentation," in *MICCAI*, 2015.
- [58] Q. Fan, D.-P. Fan, H. Fu, C.-K. Tang, L. Shao, and Y.-W. Tai, "Group collaborative learning for co-salient object detection," in *IEEE CVPR*, 2021.
- [59] Z. Zhang, W. Jin, J. Xu, and M.-M. Cheng, "Gradient-induced co-saliency detection," in *ECCV*, 2020.
- [60] Q. Hou, M.-M. Cheng, X. Hu, A. Borji, Z. Tu, and P. H. Torr, "Deeply supervised salient object detection with short connections," in *IEEE CVPR*, 2017.
- [61] N. Liu, J. Han, and M.-H. Yang, "Picanet: Learning pixel-wise contextual attention for saliency detection," in *IEEE CVPR*, 2018.
- [62] S. Chen, X. Tan, B. Wang, and X. Hu, "Reverse attention for salient object detection," in *ECCV*, 2018.
- [63] A. Borji, S. Frintrap, D. N. Sihite, and L. Itti, "Adaptive object tracking by learning background context," in *IEEE CVPRW*, 2012.
- [64] Z.-Y. Li, S. Gao, and M.-M. Cheng, "Exploring feature self-relation for self-supervised transformer," *arXiv preprint arXiv:2206.05184*, 2022.
- [65] C. Guo and L. Zhang, "A novel multiresolution spatiotemporal saliency detection model and its applications in image and video compression," *IEEE TIP*, vol. 19, no. 1, pp. 185–198, 2009.
- [66] M.-M. Cheng, F.-L. Zhang, N. J. Mitra, X. Huang, and S.-M. Hu, "Repfinder: finding approximately repeated scene elements for image editing," *ACM TOG*, vol. 29, no. 4, pp. 1–8, 2010.
- [67] A. Shaban, S. Bansal, Z. Liu, I. Essa, and B. Boots, "One-shot learning for semantic segmentation," in *BMVC*, 2017.
- [68] X. Zhang, Y. Wei, Y. Yang, and T. S. Huang, "Sg-one: Similarity guidance network for one-shot semantic segmentation," *IEEE TCYB*, vol. 50, no. 9, pp. 3855–3865, 2020.
- [69] Z. Tian, H. Zhao, M. Shu, Z. Yang, R. Li, and J. Jia, "Prior guided feature enrichment network for few-shot segmentation," *IEEE TPAMI*, vol. 44, no. 2, pp. 1050–1065, 2020.
- [70] C. Lang, G. Cheng, B. Tu, and J. Han, "Learning what not to segment: A new perspective on few-shot segmentation," in *IEEE CVPR*, 2022.
- [71] R. Li, K. Li, Y.-C. Kuo, M. Shu, X. Qi, X. Shen, and J. Jia, "Referring image segmentation via recurrent refinement networks," in *IEEE CVPR*, 2018.
- [72] C. Liu, Z. Lin, X. Shen, J. Yang, X. Lu, and A. Yuille, "Recurrent multimodal interaction for referring image segmentation," in *IEEE ICCV*, 2017.
- [73] H. Shi, H. Li, F. Meng, and Q. Wu, "Key-word-aware network for referring expression image segmentation," in *ECCV*, 2018.
- [74] Y. Zhou, R. Ji, G. Luo, X. Sun, J. Su, X. Ding, C.-W. Lin, and Q. Tian, "A real-time global inference network for one-stage referring expression comprehension," *IEEE TNNLS*, 2021.
- [75] G. Luo, Y. Zhou, X. Sun, L. Cao, C. Wu, C. Deng, and R. Ji, "Multi-task collaborative network for joint referring expression comprehension and segmentation," in *IEEE CVPR*, 2020.
- [76] X. Sun, X. Zhang, L. Cao, Y. Wu, F. Huang, and R. Ji, "Exploring language prior for mode-sensitive visual attention modeling," in *ACM MM*, 2020.
- [77] F. Perazzi, J. Pont-Tuset, B. McWilliams, L. Van Gool, M. Gross, and A. Sorkine-Hornung, "A benchmark dataset and evaluation methodology for video object segmentation," in *IEEE CVPR*, 2016.
- [78] W. Wang, J. Shen, F. Guo, M.-M. Cheng, and A. Borji, "Revisiting video saliency: A large-scale benchmark and a new model," in *IEEE CVPR*, 2018.
- [79] T.-N. Le, T. V. Nguyen, Z. Nie, M.-T. Tran, and A. Sugimoto, "Anabranch network for camouflaged object segmentation," *CVIU*, vol. 184, pp. 45–56, 2019.
- [80] Y. Lv, J. Zhang, Y. Dai, A. Li, B. Liu, N. Barnes, and D.-P. Fan, "Simultaneously localize, segment and rank the camouflaged objects," in *IEEE CVPR*, 2021.
- [81] B. Zhou, A. Lapedriza, A. Khosla, A. Oliva, and A. Torralba, "Places: A 10 million image database for scene recognition," *IEEE TPAMI*, vol. 40, no. 6, pp. 1452–1464, 2017.
- [82] K. He, X. Zhang, S. Ren, and J. Sun, "Deep residual learning for image recognition," in *IEEE CVPR*, 2016.
- [83] B. Huang, D. Lian, W. Luo, and S. Gao, "Look before you leap: Learning landmark features for one-stage visual grounding," in *IEEE CVPR*, 2021.
- [84] Z. Yang, B. Gong, L. Wang, W. Huang, D. Yu, and J. Luo, "A fast and accurate one-stage approach to visual grounding," in *IEEE ICCV*, 2019.
- [85] X. Shi, Z. Chen, H. Wang, D.-Y. Yeung, W.-K. Wong, and W.-c. Woo, "Convolutional lstm network: A machine learning approach for precipitation nowcasting," in *NeurIPS*, 2015.
- [86] M. Tan and Q. Le, "Efficientnet: Rethinking model scaling for convolutional neural networks," in *ICML*, 2019.

- [87] S.-H. Gao, M.-M. Cheng, K. Zhao, X.-Y. Zhang, M.-H. Yang, and P. Torr, "Res2net: A new multi-scale backbone architecture," *IEEE TPAMI*, vol. 43, no. 2, pp. 652–662, 2019.
- [88] Y. Jing, T. Kong, W. Wang, L. Wang, L. Li, and T. Tan, "Locate then segment: A strong pipeline for referring image segmentation," in *IEEE CVPR*, 2021.
- [89] J. Liu, Y. Bao, G.-S. Xie, H. Xiong, J.-J. Sonke, and E. Gavves, "Dynamic prototype convolution network for few-shot semantic segmentation," in *IEEE CVPR*, 2022.
- [90] J. Wei, S. Wang, and Q. Huang, "F³net: fusion, feedback and focus for salient object detection," in *AAAI*, 2020.
- [91] D. P. Kingma and J. Ba, "Adam: A method for stochastic optimization," in *ICLR*, 2015.
- [92] I. Loshchilov and F. Hutter, "Sgdr: Stochastic gradient descent with warm restarts," in *ICLR*, 2017.
- [93] A. Paszke, S. Gross, F. Massa, A. Lerer, J. Bradbury, G. Chanan, T. Killeen, Z. Lin, N. Gimelshein, L. Antiga *et al.*, "Pytorch: An imperative style, high-performance deep learning library," in *NeurIPS*, 2019.
- [94] L.-C. Chen, G. Papandreou, I. Kokkinos, K. Murphy, and A. L. Yuille, "Deeplab: Semantic image segmentation with deep convolutional nets, atrous convolution, and fully connected crfs," *IEEE TPAMI*, vol. 40, no. 4, pp. 834–848, 2017.
- [95] S. Liu, D. Huang *et al.*, "Receptive field block net for accurate and fast object detection," in *ECCV*, 2018.
- [96] A. Radford, J. W. Kim, C. Hallacy, A. Ramesh, G. Goh, S. Agarwal, G. Sastry, A. Askell, P. Mishkin, J. Clark *et al.*, "Learning transferable visual models from natural language supervision," in *ICML*, 2021.
- [97] T. Lüddecke and A. Ecker, "Image segmentation using text and image prompts," in *IEEE CVPR*, 2022.